



Flow Past of a Drilling Riser System with Auxiliary Lines in Laminar Flow

Mohd Asamudin A. Rahman^{1,2}, Fatin Alias¹, Mohd Hairil Mohd^{1,*}

¹ Maritime Technology and Naval Architecture Programme, Faculty of Ocean Engineering Technology and Informatics, Universiti Malaysia Terengganu, 21030 Kuala Nerus, Terengganu, Malaysia

² Institute of Oceanography and Environment, Universiti Malaysia Terengganu, 21030 Kuala Nerus, Terengganu, Malaysia

ARTICLE INFO

Article history:

Received 12 September 2022

Received in revised form 3 October 2022

Accepted 25 October 2022

Available online 1 February 2023

Keywords:

VIV; drilling riser; laminar; auxiliary lines; CFD

ABSTRACT

Vortex-Induced Vibration (VIV) has emerged as a crucial problem that may arise during a drilling operation, which could result in riser failure. Engineers focus on drilling riser's flow characteristics and controls with the intention of improving the drilling environment. Auxiliary lines or control rods are usually placed around the main drilling riser to suppress the VIV. However, the issue related to the flow past drilling riser system with auxiliaries has yet to be resolved. The flow characteristics around a riser system with auxiliaries were analysed in this research. The simulations were conducted using Computational Fluid Dynamics (CFD) software, Altair AcuSolve. This work focuses on the influence of various gap ratios (G/D) and diameter ratios (d/D) on the vortex interaction. A main cylinder with six auxiliary lines was modelled with G/D of 0 to 2.0 and d/D of 0.10 to 0.60 to simulate the riser system. The simulations were carried out at Reynold Number of 200 in the laminar flow regime. The results revealed that the hydrodynamic forces decreased when d/D and G/D increased. The vortex shedding was significantly reduced for auxiliary lines with G/D between 0.3 and 1.4. The numerical simulation results indicated that the vortex interaction in the wake region was, and the hydrodynamic forces were reduced due to the auxiliary lines configurations. The findings of this study are intended to contribute a new CFD simulation result for a better prediction of VIV on a drilling riser with auxiliary lines.

1. Introduction

A drilling riser is a conduit that provides a temporary connection between the underground oil wells to surface drilling facilities. It is installed in the deep sea during the development of oil and gas reserves. A riser is a pipe that links an offshore Floating Production System or a Drilling Rig to a sub-sea network for production purposes such as exploration, manufacturing, injection and export, or mining, finishing and processing purposes. Figure 1 shows the sketch of a Floating Production, Drilling, Storage and Offloading (FPDSO) [1]. Risers are regarded as the most essential component in the construction of an offshore pipeline, considering the complex loads and the harsh operating conditions that they have to withstand. However, the movement of the riser produces an equal flow that can induce Vortex-Induced Vibration (VIV) even without the current of the ocean. In recent

* Corresponding author.

E-mail address: m.hairil@umt.edu.my (Mohd Hairil Mohd)

decades, VIV has become a critical study in the field of theoretical and experimental fluid dynamics [2].

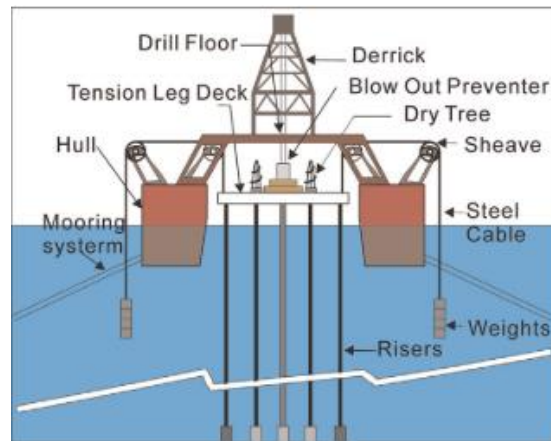


Fig. 1. Sketch of FPSO [1]

Some efforts have been done in VIV research, particularly on the prediction of vibration on offshore structures. In order to optimize the drilling operation, flow analysis and flow control must be considered. Several approaches have been suggested by Wu *et al.*, [3] to overcome VIV reactions, which include active and passive flow control methods. Active flow control method involves rotationally oscillating the feedback cylinders, whereas passive method comprises of small rods of helical strake, splitter plates and rotating circular cylinders. For example, Lou *et al.*, [4] had performed an experiment to elucidate the impact of using control rods on the suppression of VIV. It was observed that the greatest suppression was obtained when the riser was designed in a tandem arrangement. In another study, Silva-Ortega and Assi [5] identified a method that could be used to reduce drag, which involved placing control rods around the main cylinder. They conducted an experiment using a model comprising of a circular cylinder surrounded by the control rods. The experiment was conducted on a free surface channel with a Reynolds number of 5000. The authors concluded that the placement of four and eight control rods produced better results compared to that of two control rods. It was also observed that the spacing ratio of 0.05 and the diameter ratio of 0.06 produced a lower drag coefficient. In conclusion, the gap ratio, diameter ratio and positions of control rods play important roles in suppressing the VIV.

According to Strykowski and Sreenivasan [6], vortices could be suppressed when the smaller cylinder was positioned within a fixed region downstream of the main cylinder ($Re = 80$). This claim was supported by similar research done by Kuo *et al.*, [7]. They stated that the wake pattern could be changed even when the vortex-wake was formed, by placing two cylinders in the vicinity of the wake region. In addition to a VIV response, the downstream cylinder experienced a wake-induced vibration due to the interactions between vortices shed from both cylinders [8].

A recent study by, Rahman *et al.*, [9] predicted the Vortex-induced Motion (VIM) for low aspect ratios by modifying the wake oscillator model. It was found that in this research the model had successfully forecasted the VIM of floaters by changing the aspect ratios from 0.2 to 2.0 to observe the 3D phenomenon.

Besides, Gao *et al.*, [10] studied the effect of VIV on the heave movement by adjusting the added mass dependent. The rotation of the platform heave often had a major impact on the vibration modes of the riser. Each element had a distinct influence on the VIV response of the riser in the in-line and cross-flow directions. The improved model as well as the results of this research could be utilized during the installation of a marine drilling riser.

Previous studies had confirmed that VIV could be affected by the gap ratio and diameter ratio. Zhao *et al.*, [11] have conducted a numerical simulation of flow passing between one large and one small circular cylinder to study the impacts of the distance ratio between the two cylinders. They observed that if the cylinders were appropriately arranged, the hydrodynamic forces could be decreased. Vortex shedding can be classified into three modes, namely single-wake shedding mode, interaction mode and two-wake mode, where each mode was distinguished by a very small gap ratio, medium gap ratio and a very large gap ratio. As highlighted by Zhu and Yao [12], when the diameter ratio increased, the oscillations in the in-line and cross-flow directions decreased. In addition, the mean in-line displacement, the percentage of the total cross-sectional area of the cylinders, and the drag coefficient all increased as the diameter ratio varied. Based on a comprehensive strategy, the 0.15 diameter ratio was considered the optimum value.

Therefore, the design of the auxiliary line for the drilling riser is still challenging. This paper extends the study from previously published work by Lu *et al.*, [13] to study the fundamental flow over drilling riser with auxiliary lines. The significance of this study is to investigate the flow past until gap ratio of 0 and addition to diameter ratio up to 0.60. We had conducted the innovation which is investigated in freely vibrating cylinder and the research was published [14,15]. The flow analysis and control of a drilling riser system with control rods or auxiliary lines were demonstrated using the Computational Fluid Dynamics (CFD) approach. The drilling riser system was modelled as circular cylinders with various auxiliary configurations. Thus, the drag and lift reduction, as well as the wake interaction system, were the essential issues in fluid flow research beyond the numerous circular cylinders. The Reynold number, $Re = 200$ was used in the simulation, which corresponded to the laminar flow regime.

2. Methodology

2.1 Governing Equations

2.1.1 Continuity equation

The instantaneous mass conservation equation commonly termed as the continuity equation, is derived by applying mass conservation to a control volume for a general fluid as shown in Eq. (1).

Its differential form is written as:

$$\frac{\partial \rho}{\partial t} + \nabla \cdot (\rho \vec{u}) = 0 \quad (1)$$

Where,

ρ is the fluid density

t is time

\vec{u} is the flow velocity vector

The first term $\frac{\partial \rho}{\partial t}$ describes the rate of change of density with respect to time and the second term $\nabla \cdot (\rho \vec{u})$ describes the divergence of the vector field $\rho \vec{u}$ at a particular point fixed in space. The continuity equation can also be expressed using the substantial derivative and is written as Eq. (2):

$$\frac{D\rho}{Dt} + \nabla \cdot (\rho \vec{u}) = 0 \quad (2)$$

2.2 Computational Model and Boundary Conditions

In this study, the drilling riser was modelled as a circular cylinder. Six identical circular cylinders were located around the main cylinder at a specific distance, as shown in Figure 2. Gap ratio (G/D) and diameter ratio (d/D) were defined as in Eq. (3) and Eq. (4), where G is the gap or distance between the surface of the main cylinder and the surface of each auxiliary line. D is the diameter of the main cylinder while d is the diameter of the auxiliary line. The range of the gap ratio was between 0 and 2, and the range of the diameter ratio was between 0.1 and 0.6. Physical parameter values utilized in the present study are presented in Table 1.

The boundary conditions of the domain are tabulated in Table 2. At the inlet boundary, the mean velocity of the uniform flow corresponded to Reynold Number of 200. Slip wall was assigned to the wall boundaries to simulate the boundaries of the pressure outlet where there was no shear stress between the fluid and the walls. Finally, no viscous stress was considered at the outlet. It should be noted that the time step was 0.05s, within which the solution could adequately be stabilized.

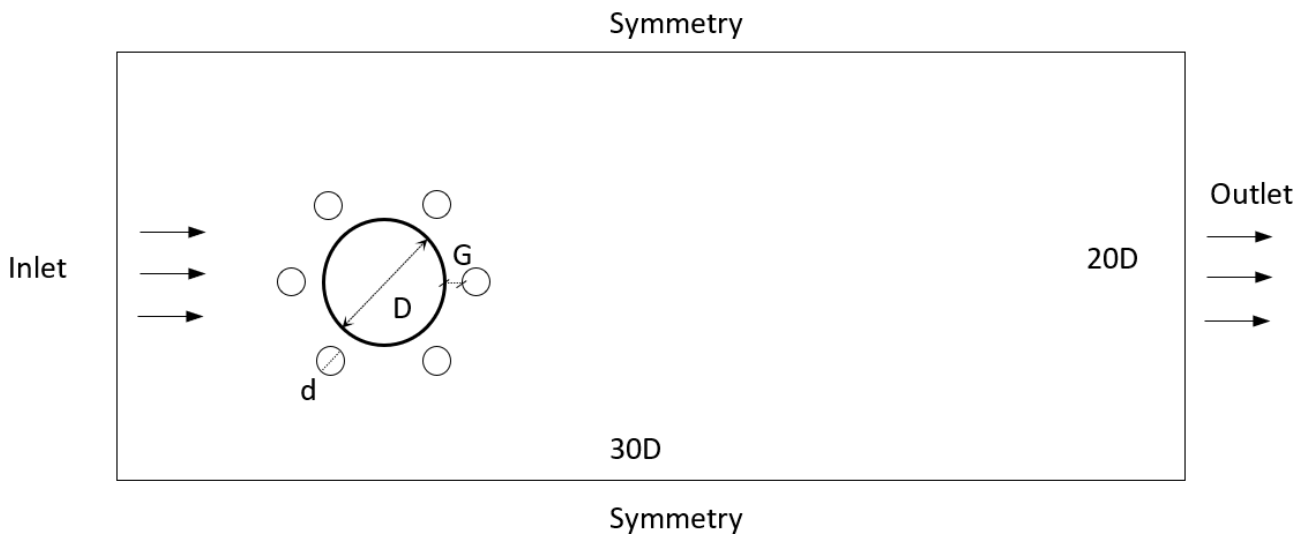


Fig. 2. Configuration for a main cylinder and six identical auxiliary lines

Table 1

Physical Parameter Values

Parameter	Symbol	Value
Gap ratio	$\frac{G}{D}$	0 – 2
Diameter ratio	$\frac{d}{D}$	0.1-0.6
Reynold Number	-	200
Mass ratio	m^*	2.0
Damping	ζ	0.007

$$\text{Gap ratio, } = \frac{G}{D} \tag{3}$$

$$\text{Diameter ratio, } = \frac{d}{D} \tag{4}$$

Table 2
 The boundary conditions of the CFD model

Type of boundary	Surface Name
Wall	Main cylinder, auxiliaries
Symmetry	Top, Bottom, Sides
Inflow	Inlet
Outflow	Outlet

2.3 Mesh Independence Study of Drilling Riser

Two mesh independent studies were conducted to obtain a stable solution for the numerical models, namely (1) a single cylinder and (2) a main cylinder with six auxiliary lines.

2.3.1 A single cylinder

Figure 3 shows a graph of the number of mesh elements plotted against the mean drag coefficient for the mesh independent study. The number of mesh elements had a significant effect on the results. It can be seen that the mean drag coefficient reached a steady-state after 66 214 elements. The mean drag coefficient of 1.3500 was determined from the graph after it reached steady-state and it was consistent with the mean drag coefficient value reported by Braza *et al.*, [16].

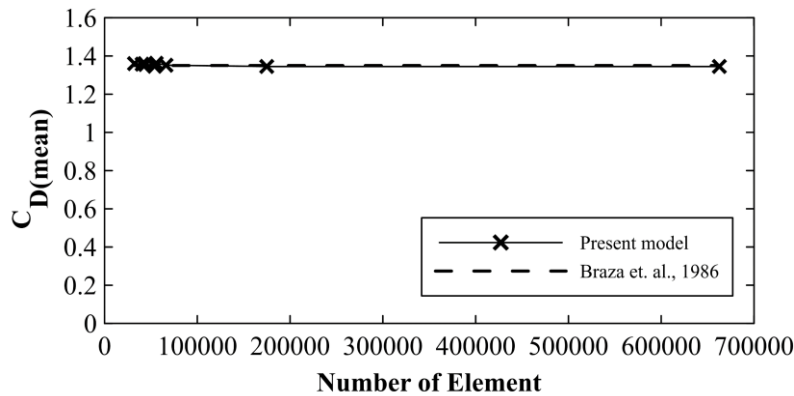


Fig. 3. Mesh independent study for a single cylinder with different mesh qualities

2.3.2 A main cylinder with six auxiliary lines

Nine mesh independent studies were conducted by varying the absolute mesh size within the range of 0.01m to 0.09m. Figure 4 shows the graph of the number of elements against the mean drag coefficient for the convergence test. The results were consistent, where the mean drag coefficient $C_{D(mean)} = 1.74747$ was approximately 1.74747 at 65 592 elements. Figure 5 illustrates the mesh configurations for the simulation domain.

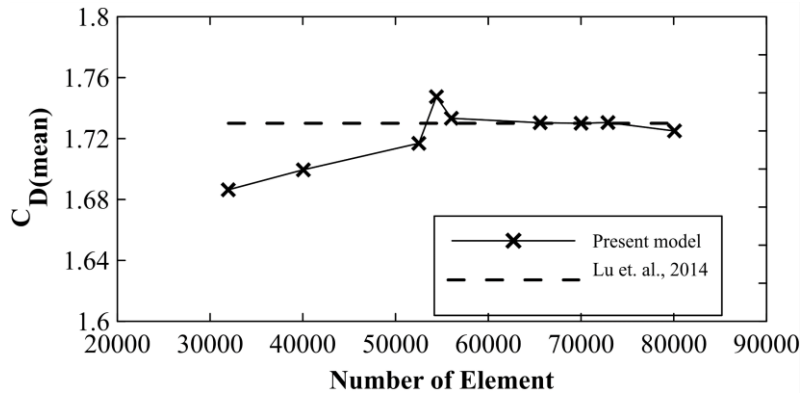


Fig. 4. Mesh independent studies for a main cylinder and six auxiliary lines with different mesh qualities

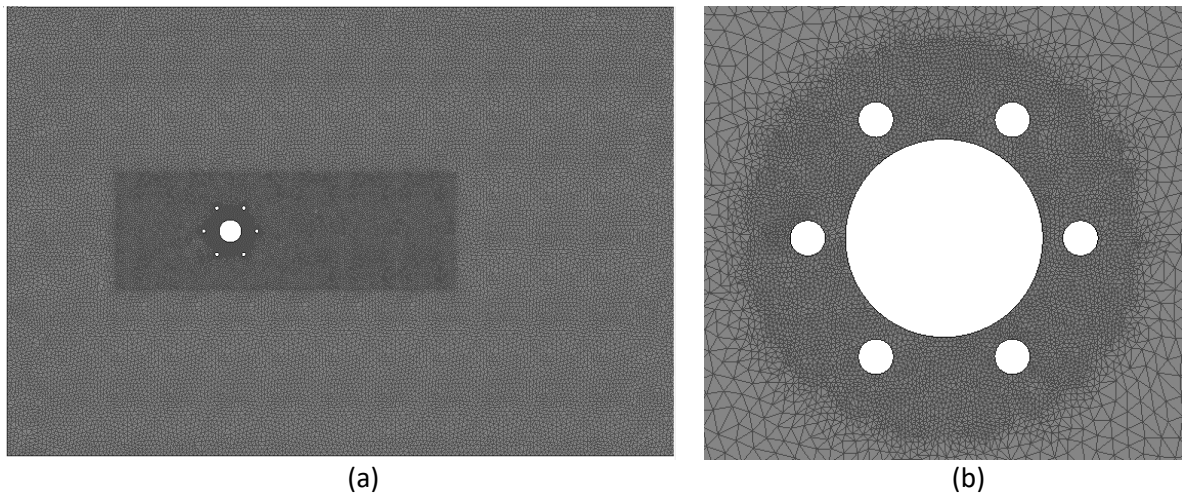


Fig. 5. (a) Computation domain meshes of a main cylinder with six auxiliary lines. (b) Illustration of the mesh for case $d/D= 0.10$ and $G/D = 0.08$

2.4 Model Validation

The model validation was conducted in order to verify and check the current CFD model's validity and dependability.

2.4.1 Model validation of a single cylinder

The Mean Drag Coefficient and Strouhal Number for a single fixed cylinder at $Re = 200$ were determined. Then, the results were compared to published data to validate the computational method. Table 3 lists down the results for the present model together with the data from three published literature, namely Braza *et al.*, [16], Meneghini *et al.*, [17] and Arkell [18]. The mean drag coefficient for the present model was 1.385697, which was slightly higher than the numerical simulation reported in the papers. On the other hand, the Strouhal number of 0.19660 obtained from the present simulation was equal to the numerical simulations by Meneghini *et al.*, [17] and Arkell [18] which was 0.19600 but was slightly lower than that reported by Braza *et al.*, [16] which was 0.20000.

Table 3
 Mean Drag Coefficient and Strouhal Numbers of a single cylinder at Re = 200

	St	Mean Drag Coefficient
Present	0.19660	1.385697
Meneghini & Saltara (2001)	0.19600	1.300000
Braza <i>et al.</i> , (1986)	0.20000	1.350000
Arkell (1995)	0.19600	1.300000

2.4.2 Model validation of a main cylinder with six auxiliary lines

The numerical results associated with the model comprised of one main cylinder and six auxiliary lines are presented. A rectangular computational domain of 20D and 30D was determined from a domain-size independent study. As a result, Figure 6 shows the mean drag coefficient and rms lift coefficient of Lu *et al.*, [13] and the present simulation for d/D=0.1, 0.18, 0.24, 0.30 and 0.35 with Re= 200, respectively. Based on the results obtained, it can be seen that the simulations were in good agreement with published data and the fell within the accepted range. The maximum relative error was less than 10%.

The numerical findings indicated that the connected auxiliary lines may substantially reduce the fluid forces on the main cylinder. The drag coefficient (C_D) and Lift coefficient (C_L) were calculated as per Eq. (5) and Eq. (6) [3].

$$C_D = \frac{2F_x}{\rho U^2 D} \tag{5}$$

$$C_L = \frac{2F_y}{\rho U^2 D} \tag{6}$$

Where F_x and F_y are fluid forces in the in-line and the cross-flow directions respectively, ρ is the density of the fluid, U is the time-average velocity vector of the fluid and D is the main diameter of the main cylinder. Meanwhile, the mean drag coefficient (C_{D (mean)}) and root mean square (rms) lift coefficient (C_{L (rms)}) were calculated using Eq. (7) and Eq. (8).

$$C_{D (mean)} = \frac{1}{N} \sum_{n=1}^N C_D \tag{7}$$

$$C_{L (rms)} = \sqrt{\frac{1}{N} \sum_{n=1}^N (C_L - \overline{C_L})^2} \tag{8}$$

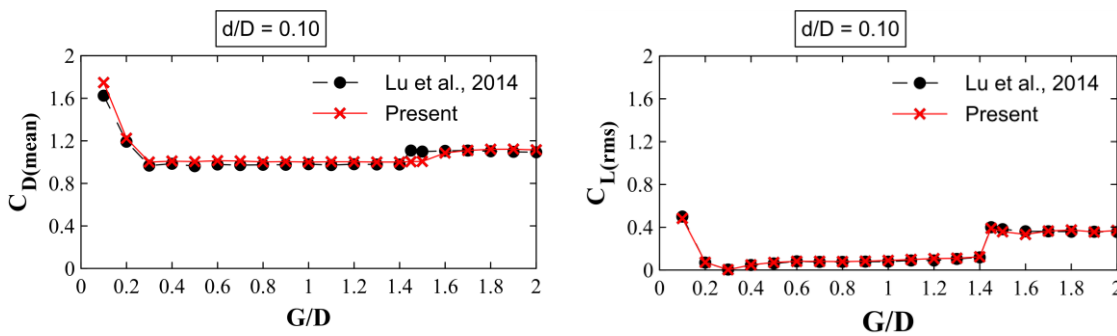


Fig. 6. Comparison and validation between Lu *et al.*, [13] and present model for mean drag coefficient and rms lift coefficient of a main cylinder and six auxiliary lines at Re = 200

3. Results

In order to simplify the discussion of the results, the gap ratio was divided into five regimes as shown in Table 4. The selection of the regime was based on the characteristics of the hydrodynamic forces at various gap ratios. Figure 7 shows the result of mean drag coefficient for $d/D = 0.10$ to 0.60 and $G/D = 0$ to 2.0 . The simulations were conducted using a main cylinder and six auxiliary lines model.

Table 4

Range of Regime	
Regime	Range
1	$0 \leq G/D \leq 0.1$
2	$0.1 < G/D \leq 0.3$
3	$0.3 < G/D \leq 1.4$
4	$1.4 < G/D < 1.5$
5	$G/D \geq 1.5$

For Regime 1, the mean drag coefficient increased rapidly for $G/D = 0, 0.02, 0.04, 0.06, 0.08$ and 0.1 . As seen from the plot, the maximum value of $C_{D (mean)}$ was 1.84850 at $G/D = 0.06$ and $d/D = 0.35$. This was due to the presence of stagnation pressure at the front of the cylinder and the high pressure that increased the drag. The pattern of wake as shown in Figure 7 confirmed this finding.

In Regime 2, the $C_{D (mean)}$ decreased significantly when G/D was increased and it converged at 1.00010 when $G/D = 0.3$. The decreased in $C_{D (mean)}$ was observed on the main cylinder when the auxiliary line was near, which was caused by a separation point along the surfaces of the main cylinder. The findings were consistent with the study by Silva-Ortega and Assi [19]. It was discovered that the gap ratio had significant effect on the results of $C_{D (mean)}$, in which, the higher the gap ratio, the lower the drag force. For Regime 3, the $C_{D (mean)}$ continued to decrease as G/D increased.

A slightly lower value of $C_{D (mean)} = 0.70403$ was obtained from the plot at $G/D = 1.3$ and $d/D = 0.50$. This was resulted from the increase in basic pressure, which was due to the disturbance from the small cylinders of the upper cylinder formation and the interactions between the shear layers of the main cylinder.

Next, in Regime 4, a different trend was observed where $C_{D (mean)}$ increased as G/D increased. It can be observed that the highest $C_{D (mean)}$ value of 1.0048 was obtained when $d/D = 0.10$. The unstable drag values was probably due to the beat of motion in the time series acquired in the simulations. Nevertheless, the values of $C_{D (mean)}$ were within the accepted range.

Finally, in Regime 5, it can be seen that the smaller the d/D , the higher the $C_{D (mean)}$. The highest $C_{D (mean)}$ was obtained at d/D of 0.10 . This was similar to the trend observed in Regime 4 in which the smaller d/D , the higher the $C_{D (mean)}$ on the main cylinder. The presence of the auxiliary lines close to the main cylinder prevented the vortices from interacting across the centre line of the wake, which affected the $C_{D (mean)}$ of the main cylinder. This finding was supported by the report from Song *et al.*, [20] which revealed that the maximum suppression occurred when three auxiliary lines were placed at gap ratio of 0.9 . Their results show that the three auxiliaries were more efficient than one auxiliary when it comes to suppressing the VIV when the gap ratio is less than 1.0 .

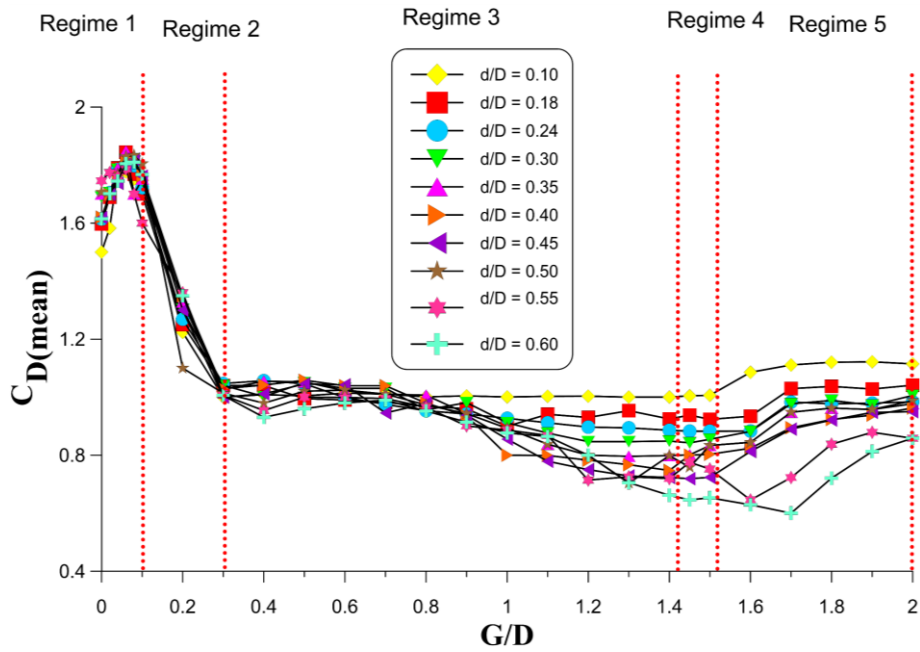


Fig. 7. Mean Drag Coefficient with different gap ratios

The results for $C_{L(rms)}$ for $d/D = 0.10 - 0.50$ and $G/D = 0 - 2.0$ are shown in Figure 8. The discussion of the results begins with Regime 1, where the rms lift coefficient increased significantly for all G/D . The $C_{L(rms)}$ reached its maximum value of 0.68841 at $d/D = 0.3$ as well as $G/D = 0.06$. The development of the shear layers on the upstream face of the main cylinder and the interaction between the shear layers in the wake area of the main cylinder was disrupted by the six auxiliary lines.

In Regime 2, the $C_{L(rms)}$ reduced steeply then converges close to zero at $G/D = 0.2$ and 0.3 . The average of $C_{L(rms)}$ when $G/D = 0.10$ is 0.49975. Meanwhile, the average lift coefficient when $G/D = 0.20$ is 0.14750. This shows that a large amount is decreasing of $C_{L(rms)}$.

A significant reduction in $C_{L(rms)}$ can be seen in the Regime 3. The minimum $C_{L(rms)}$ observed was 0.00060 at $G/D = 0.40$ and $d/D = 0.18$. The presence of six auxiliary lines in the wake of the main cylinder caused the shear layers behind the main cylinder to interact afterwards.

Meanwhile, $C_{L(rms)}$ was observed to experience an increase in Regime 4. At $d/D = 1.4$, $C_{L(rms)}$ started to ascend until it reached the highest value of 0.39012 at $d/D = 0.10$. Lastly, in Regime 5, $C_{L(rms)}$ decreased gradually as G/D increased. The highest $C_{L(rms)}$ recorded was at $d/D=0.45$. Unlike $C_{D(mean)}$, the effect of the d/D on $C_{L(rms)}$ was found to be very minimal. The finding revealed that the lower the G/D , the higher the rms lift coefficient due to the shedding of the vortices. As reported by Zhu and Yao [12] at a low diameter ratio, the hydrodynamic forces and motion responses had essentially constant amplitudes. When the diameter ratio was increased, the mean drag coefficient improved significantly. The rms lift coefficient, on the other hand, appeared to decrease as the diameter ratio increased. Furthermore, the force component that acted on the main cylinder predominated the total force coefficient. The overall rms force coefficient varied similarly to that of the main cylinder. This statement is in accordance with the findings from Wang *et al.*, [21], where the mean drag coefficient decreased approximately 10% to 31% and the rms lift coefficient decreased 30% to 99% for all faired systems at given bare cylinder.

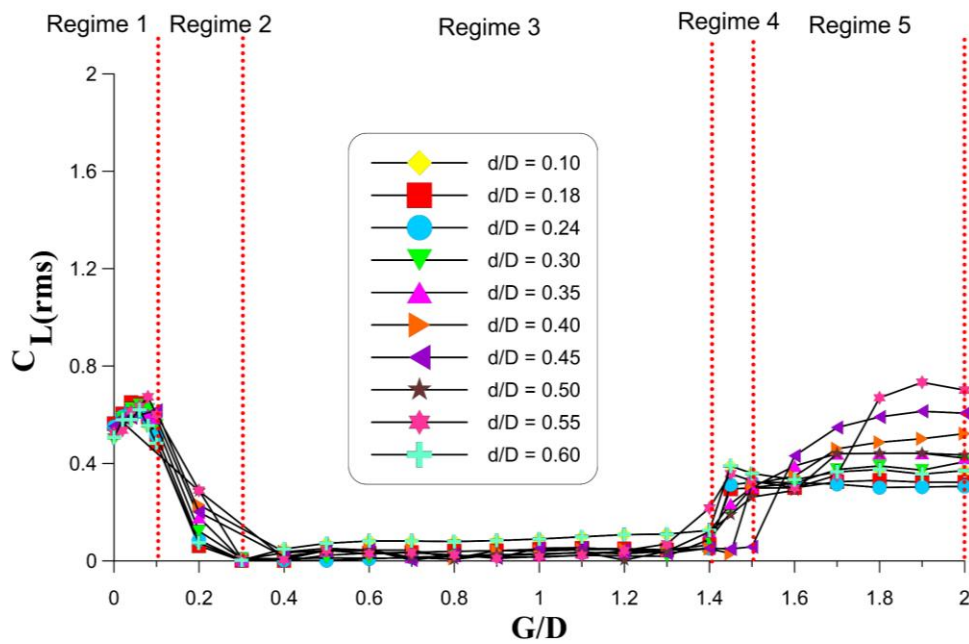
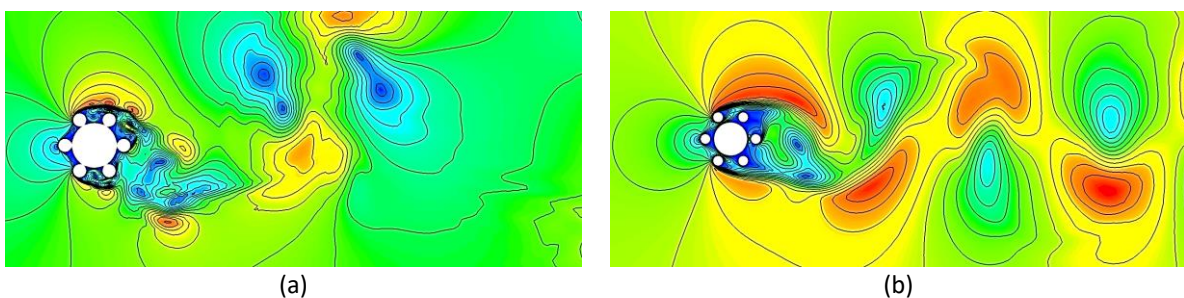


Fig. 8. rms Lift Coefficient with different gap ratios

Figure 9 illustrates the contour in velocity magnitude for $d/D = 0.30$ and $G/D = 0, 0.04, 0.10, 0.50, 1.00$ and 2.00 . By comparing $G/D = 0, 0.04$ and 0.10 , it was proven that the installation of several control rods with a very low gap ratio helped in maintaining the flow pattern in the close wake. The recognized alternating vortex shedding and even *Kármán Vortex Street* are obtained. The increase in the vortex size and the vortex shedding period depended on the diameter ratio and gap ratio. At higher gap ratios, the vortices shedding behind the small cylinder were weaker than those shedding behind the main cylinder, which was in agreement with Zhu and Gao [22]. This was due to the force component of the main cylinder being dominant in the total force coefficient. It should be noted here, the elimination of flow separation along the rear surface and the merging of the two-gap streams toward the wake centrelines of the main cylinder largely reduce the wake width, as mentioned by Wang and Zhao [23].

At $G/D = 0.50$ and 1.00 , three vortex streets were recognized. The three classes of vortices seemed to be dispersed independently. Additionally, it can be observed that there were strong interactions among the streets. The three vortex shedding were in phase with each other and this led to a large rms lift coefficient. Lu *et al.*, [13] also presented similar findings, in which three vortex streets appeared as a result of an increased gap ratio.

For $G/D = 2.00$, the lift amplitude increased as the gap ratio increased. Therefore, the vortex shedding took place in the close wake of the main cylinder. In addition, the results in Regime 4 were similar to those in Regime 3. However, the flow pattern was more complicated and had stronger vortex interaction. It can be concluded that the hydrodynamic forces of the main cylinder depended on flow instability and wake modes.



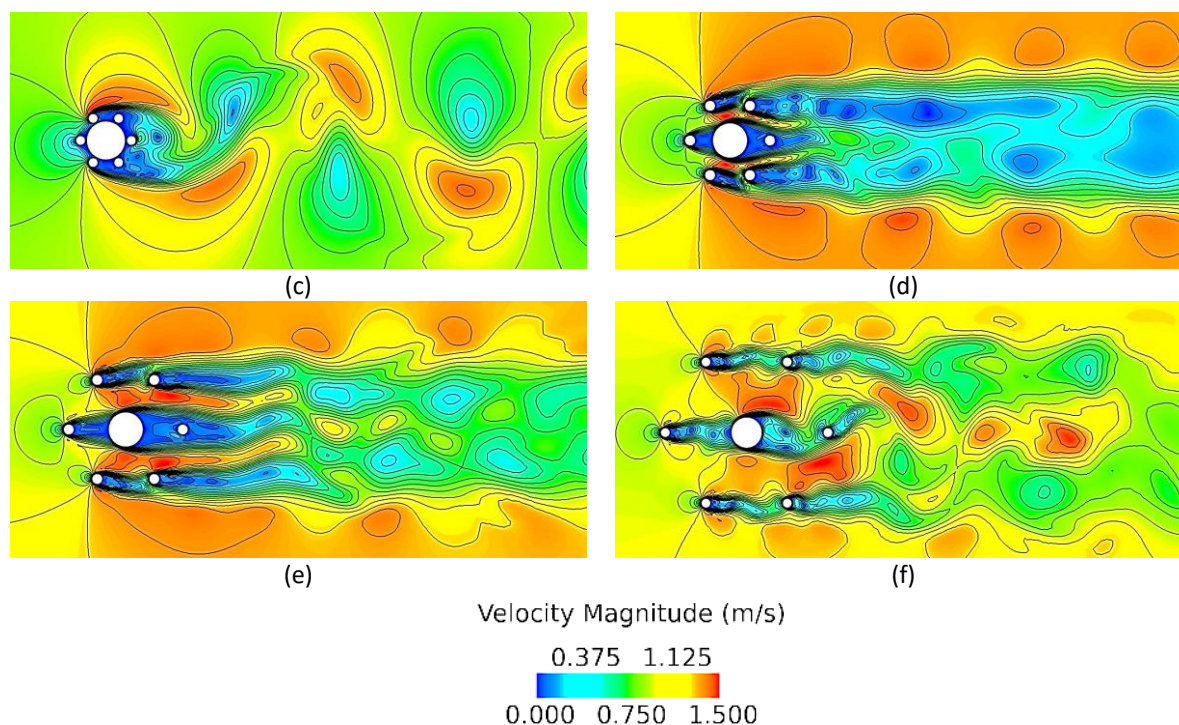


Fig. 9. Streamline around a main cylinder and six auxiliary lines under diameter ratio = 0.30 in varying gap ratio; (a) 0, (b) 0.04, (c) 0.10, (d) 0.50, (e) 1.00, (f) 2.00

4. Conclusions

This present study was designed to determine the effects of the gap and the diameter ratios of a drilling riser with auxiliaries on the vortex shedding phenomenon. This study has shown that five flow regimes can be identified by varying the gap and diameter ratios at $Re = 200$. It was found that in Regime 1, both mean drag and rms lift coefficients were increased. However, the hydrodynamic coefficients decreased when the gap ratio was increased in Regime 2 and 3. The mean drag and rms lift coefficients exhibited a significantly high value in Regime 4 as the gap ratio was further increased. Meanwhile, in Regime 5, the vortex shedding phenomenon independently occurred and was not affected by the auxiliary lines. The results of this investigation revealed that the drag and lift components were reduced within the gap ratio range of $0.3 < G/D < 1.4$. In addition, larger diameter ratios between the range of $0.35 < d/D < 0.60$ resulted in a significant reduction of the mean drag component, similar to that in the gap ratio range. Taken together, these gap and diameter ratios can be considered as the optimum values for the design of drilling riser with auxiliary lines in order to reduce the vortex shedding phenomenon on the main drilling riser.

Acknowledgement

This research was funded by Ministry of Higher Education of Malaysia (Award No. FRGS/1/2022/TK06/UMT/02/7, Vot No. 59713).

References

- [1] Zhang, Wen-Shou, and Dong-Dong Li. "Active control of axial dynamic response of deepwater risers with Linear Quadratic Gaussian controllers." *Ocean Engineering* 109 (2015): 320-329. <https://doi.org/10.1016/j.oceaneng.2015.09.018>
- [2] Lee, Abe H., Robert L. Campbell, and Stephen A. Hambric. "Coupled delayed-detached-eddy simulation and structural vibration of a self-oscillating cylinder due to vortex-shedding." *Journal of Fluids and Structures* 48 (2014):

- 216-234. <https://doi.org/10.1016/j.jfluidstructs.2014.02.019>
- [3] Wu, Wenbo, Jiasong Wang, Shiquan Jiang, Liangbin Xu, and Leixiang Sheng. "Flow and flow control modeling for a drilling riser system with auxiliary lines." *Ocean Engineering* 123 (2016): 204-222. <https://doi.org/10.1016/j.oceaneng.2016.06.043>
- [4] Lou, Min, Wu-gang Wu, and Peng Chen. "Experimental study on vortex induced vibration of risers with fairing considering wake interference." *International Journal of Naval Architecture and Ocean Engineering* 9, no. 2 (2017): 127-134. <https://doi.org/10.1016/j.ijnaoe.2016.08.006>
- [5] Silva-Ortega, M., and G. R. S. Assi. "Flow-induced vibration of a circular cylinder surrounded by two, four and eight wake-control cylinders." *Experimental Thermal and Fluid Science* 85 (2017): 354-362. <https://doi.org/10.1016/j.expthermflusci.2017.03.020>
- [6] Strykowski, P. J., and K. R. Sreenivasan. "On the formation and suppression of vortex 'shedding' at low Reynolds numbers." *Journal of Fluid Mechanics* 218 (1990): 71-107. <https://doi.org/10.1017/S0022112090000933>
- [7] Kuo, C-H., L-C. Chiou, and C-C. Chen. "Wake flow pattern modified by small control cylinders at low Reynolds number." *Journal of Fluids and Structures* 23, no. 6 (2007): 938-956. <https://doi.org/10.1016/j.jfluidstructs.2007.01.002>
- [8] Bearman, P. W. "Circular cylinder wakes and vortex-induced vibrations." *Journal of Fluids and Structures* 27, no. 5-6 (2011): 648-658. <https://doi.org/10.1016/j.jfluidstructs.2011.03.021>
- [9] Rahman, Mohd Asamudin A., Wan Norazam Wan Hussin, Mohd Hairil Mohd, Fatimah Noor Harun, Lee Kee Quen, and Jeom Kee Paik. "Modified wake oscillator model for vortex-induced motion prediction of low aspect ratio structures." *Ships and Offshore Structures* 14, no. sup1 (2019): 335-343. <https://doi.org/10.1080/17445302.2019.1593308>
- [10] Gao, Guanghai, Xiao Cong, Yunjing Cui, and Xingqi Qiu. "Study on vortex-induced vibration of deep-water marine drilling risers in linearly sheared flows in consideration of changing added mass." *Mathematical Problems in Engineering* 2020 (2020). <https://doi.org/10.1155/2020/7687280>
- [11] Zhao, Ming, Liang Cheng, Bin Teng, and Dongfang Liang. "Numerical simulation of viscous flow past two circular cylinders of different diameters." *Applied Ocean Research* 27, no. 1 (2005): 39-55. <https://doi.org/10.1016/j.apor.2004.10.002>
- [12] Zhu, Hongjun, and Jie Yao. "Numerical evaluation of passive control of VIV by small control rods." *Applied Ocean Research* 51 (2015): 93-116. <https://doi.org/10.1016/j.apor.2015.03.003>
- [13] Lu, Lin, Ming-ming Liu, Bin Teng, Zhen-dong Cui, Guo-qiang Tang, Ming Zhao, and Liang Cheng. "Numerical investigation of fluid flow past circular cylinder with multiple control rods at low Reynolds number." *Journal of Fluids and Structures* 48 (2014): 235-259. <https://doi.org/10.1016/j.jfluidstructs.2014.03.006>
- [14] Alias, Fatin, Mohd Hairil Mohd, Mohd Azlan Musa, Erwan Hafizi Kasiman, and Mohd Asamudin A. Rahman. "Flow Past a Fixed and Freely Vibrating Drilling Riser System with Auxiliaries in Laminar Flow." *Journal of Advanced Research in Fluid Mechanics and Thermal Sciences* 87, no. 3 (2021): 94-104. <https://doi.org/10.37934/arfmts.87.3.94104>
- [15] Alias, Fatin, Mohd Hairil Mohd, and Mohd Asamudin A. Rahman. "The Influence of Incidence Angles on Flow Past a Fixed and Freely Vibrating Drilling Riser System in Laminar Flow." In *The 31st International Ocean and Polar Engineering Conference*. OnePetro, 2021.
- [16] Braza, M., P. H. H. M. Chassaing, and H. Ha Minh. "Numerical study and physical analysis of the pressure and velocity fields in the near wake of a circular cylinder." *Journal of Fluid Mechanics* 165 (1986): 79-130. <https://doi.org/10.1017/S0022112086003014>
- [17] Meneghini, Julio R., Fábio Saltara, Cesareo de La Rosa Siqueira, and J. A. Ferrari Jr. "Numerical simulation of flow interference between two circular cylinders in tandem and side-by-side arrangements." *Journal of Fluids and Structures* 15, no. 2 (2001): 327-350. <https://doi.org/10.1006/jfls.2000.0343>
- [18] Arkell, Richard Henry. "Wake dynamics of cylinders encountering free surface gravity waves." *PhD diss., University of London, UK*, 1995.
- [19] Silva-Ortega, M., and Gustavo Roque da Silva Assi. "Hydrodynamic loads on a circular cylinder surrounded by two, four and eight wake-control cylinders." *Ocean Engineering* 153 (2018): 345-352. <https://doi.org/10.1016/j.oceaneng.2018.01.116>
- [20] Song, Zhenhua, Menglan Duan, and Jijun Gu. "Numerical investigation on the suppression of VIV for a circular cylinder by three small control rods." *Applied Ocean Research* 64 (2017): 169-183. <https://doi.org/10.1016/j.apor.2017.03.001>
- [21] Wang, Jiasong, Hanxu Zheng, and Zhongxu Tian. "Numerical simulation with a TVD-FVM method for circular cylinder wake control by a fairing." *Journal of Fluids and Structures* 57 (2015): 15-31. <https://doi.org/10.1016/j.jfluidstructs.2015.05.008>
- [22] Zhu, Hongjun, and Yue Gao. "Effect of gap on the vortex-induced vibration suppression of a circular cylinder using

- two rotating rods." *Ships and Offshore Structures* 13, no. 2 (2018): 119-131. <https://doi.org/10.1080/17445302.2017.1328756>
- [23] Wang, Z. J., and Y. Zhou. "Vortex interactions in a two side-by-side cylinder near-wake." *International Journal of Heat and Fluid Flow* 26, no. 3 (2005): 362-377. <https://doi.org/10.1016/j.ijheatfluidflow.2004.10.006>